

## Nitric Oxide-dependent Generation of Reactive Species in Sickle Cell Disease

ACTIN TYROSINE NITRATION INDUCES DEFECTIVE CYTOSKELETAL POLYMERIZATION\*

Received for publication, August 30, 2002

Published, JBC Papers in Press, October 24, 2002, DOI 10.1074/jbc.M208916200

Mutay Aslan<sup>‡§¶||</sup>, Thomas M. Ryan<sup>§||</sup>, Tim M. Townes<sup>§||</sup>, Lori Coward<sup>\*\*</sup>, Marion C. Kirk<sup>\*\*</sup>, Stephen Barnes<sup>§\*\*‡‡</sup>, C. Bruce Alexander<sup>§§</sup>, Steven S. Rosenfeld<sup>¶||</sup>, and Bruce A. Freeman<sup>‡§¶|| ||</sup>

From the Departments of <sup>‡</sup>Anesthesiology, <sup>§</sup>Biochemistry and Molecular Genetics, <sup>§§</sup>Pathology, <sup>‡‡</sup>Pharmacology and Toxicology, <sup>¶¶</sup>Neurology, <sup>¶</sup>Center for Free Radical Biology, <sup>||</sup>Comprehensive Sickle Cell Disease Center, and <sup>\*\*</sup>Comprehensive Cancer Center Mass Spectrometry Shared Facility, University of Alabama at Birmingham, Birmingham, Alabama 35233

The intermittent vascular occlusion occurring in sickle cell disease (SCD) leads to ischemia-reperfusion injury and activation of inflammatory processes including enhanced production of reactive oxygen species and increased expression of inducible nitric-oxide synthase (NOS2). Appreciating that impaired nitric oxide-dependent vascular function and the concomitant formation of oxidizing and nitrating species occur in concert with increased rates of tissue reactive oxygen species production, liver and kidney NOS2 expression, tissue 3-nitrotyrosine (NO<sub>2</sub>Tyr) formation and apoptosis were evaluated in human SCD tissues and a murine model of SCD. Liver and kidney NOS2 expression and NO<sub>2</sub>Tyr immunoreactivity were significantly increased in SCD mice and humans, but not in nondiseased tissues. TdT-mediated nick end-label (TUNEL) staining showed apoptotic cells in regions expressing elevated levels of NOS2 and NO<sub>2</sub>Tyr in all SCD tissues. Gas chromatography mass spectrometry analysis revealed increased plasma protein NO<sub>2</sub>Tyr content and increased levels of hepatic and renal protein NO<sub>2</sub>Tyr derivatives in SCD (21.4 ± 2.6 and 37.5 ± 7.8 ng/mg) versus wild type mice (8.2 ± 2.2 and 10 ± 1.2 ng/mg), respectively. Western blot analysis and immunoprecipitation of SCD mouse liver and kidney proteins revealed one principal NO<sub>2</sub>Tyr-containing protein of 42 kDa, compared with controls. Enzymatic in-gel digestion and MALDI-TOF mass spectrometry identified this nitrated protein as actin. Electrospray ionization and fragment analysis by tandem mass spectrometry revealed that 3 of 15 actin tyrosine residues are nitrated (Tyr<sup>91</sup>, Tyr<sup>198</sup>, and Tyr<sup>240</sup>) at positions that significantly modify actin assembly. Confocal microscopy of SCD human and mouse tissues revealed that nitration led to morphologically distinct disorganization of filamentous actin. In aggregate, we have observed that the hemoglobin point mutation of sickle cell disease that mediates hemoglobin polymerization defects is translated, via inflammatory oxidant reactions, into defective cytoskeletal polymerization.

The intermittent vascular occlusion occurring in SCD<sup>1</sup> is characterized by acute, painful crises and leads to the renal and hepatic tissue injury and dysfunction manifested by patients with this hemoglobinopathy (1–3). Peripheral vascular insufficiency, accompanied by periodic restoration of blood flow, places ischemic organs at risk of additional injury by inducing a proinflammatory state reflected by enhanced superoxide (O<sub>2</sub><sup>-</sup>) and hydrogen peroxide (H<sub>2</sub>O<sub>2</sub>) generation (4–7). These reactive species, derived from xanthine oxidase (8), autoxidation of mitochondrial respiratory chain components (9), and activated neutrophils (10, 11), serve to impair NO-dependent vascular function and further activate tissue inflammatory responses (12–14). Increased expression of NOS2 and a consequent increase in tissue nitrite and nitrate (NO<sub>2</sub><sup>-</sup> + NO<sub>3</sub><sup>-</sup>) production occurs in cardiac, liver, and kidney ischemia-reperfusion (15–18). In many instances, NOS2 inhibition by arginine analogs or ablation of NOS2 gene expression significantly limits tissue ischemia-reperfusion injury (19–21). Moreover, NOS2 can serve as a locus for tissue O<sub>2</sub><sup>-</sup> production during conditions of low arginine substrate availability, as observed in SCD (22, 23). This setting favors the generation of peroxynitrite (ONOO<sup>-</sup>), the nitrating and oxidizing species produced by the radical-radical reaction of O<sub>2</sub><sup>-</sup> and NO (24).

Increased rates of production of reactive oxygen- and nitrogen-derived species in tissues mediate the oxidation and nitration of lipids, nucleotides, and susceptible protein amino acid residues. These products also suggest an impairment of biomolecular structure and function. For example, the protein nitration product NO<sub>2</sub>Tyr is elevated in a variety of inflammatory diseases mediated in part by reactive inflammatory mediators, including atherosclerosis (25), acute lung injury (26), adult respiratory distress syndrome (27), biliary cirrhosis (28), myocardial inflammation (29), ileitis (30), rheumatoid arthritis (31), endotoxin-induced kidney injury (32), chronic renal allograft rejection (33), Alzheimer's disease (34), amyotrophic lateral sclerosis (35), and sepsis (36). The development of a causal relationship between post-translational protein nitration and impaired tissue function is presently limited by insight into where and how the inflammatory modification of specific protein amino acid residues occurs *in vivo* and how this

\* This work was supported by National Institutes of Health Grants RO1-HL64937, RO1-HL58115, and P6-HL58418. The costs of publication of this article were defrayed in part by the payment of page charges. This article must therefore be hereby marked "advertisement" in accordance with 18 U.S.C. Section 1734 solely to indicate this fact.

|| To whom correspondence should be addressed: Dept. of Anesthesiology, Biomedical Research Bldg. II, 901 19th Street So., University of Alabama at Birmingham, Birmingham, AL 35233. Tel.: 205-934-4234; Fax: 205-934-7437; E-mail: Bruce.Freeman@ccc.uab.edu.

<sup>1</sup> The abbreviations used are: SCD, sickle cell disease; MS, mass spectrometry; NOS2, inducible nitric-oxide synthase; MALDI-TOF, matrix-assisted laser desorption ionization-time of flight; NO<sub>2</sub><sup>-</sup>, nitrite; NO<sub>3</sub><sup>-</sup>, nitrate; NO, nitric oxide; NO<sub>2</sub>, nitrite; ONOO<sup>-</sup>, peroxynitrite; O<sub>2</sub><sup>-</sup>, superoxide; NO<sub>2</sub>Tyr, 3-nitrotyrosine; TUNEL, TdT-mediated nick end-label; HPLC, high pressure liquid chromatography; MS/MS, tandem mass spectrometry.

is linked with biomolecule dysfunction. Herein, a combination of clinical and knockout-transgenic mouse studies underscores the extensive occurrence of NO-mediated oxidative inflammatory reactions in SCD, with actin identified as a key target for protein nitration in kidney and liver. This identification of actin as a key tissue target for protein nitration and its impaired polymerization properties reveals the significance of this post-translational protein modification in the physiopathology of SCD and related vascular inflammatory processes.

#### MATERIALS AND METHODS

**Immunofluorescence Microscopy and TUNEL Analysis**—Paraffin-embedded kidney and liver sections were obtained from SCD human autopsy samples and knockout-transgenic SCD mice (37) following approval by the Institutional Review Board for Human Use and the Institutional Animal Care and Use Committee at the University of Alabama at Birmingham. Paraffin-embedded sections were mounted on slides, deparaffinized, and processed for immunofluorescence. Primary antibody incubations were for 60 min at 25 °C using a rabbit polyclonal anti-NO<sub>2</sub>Tyr (Cayman, 5 μg ml<sup>-1</sup>) and anti-NOS2 (BD Transduction Laboratories, 16 μg ml<sup>-1</sup>). The secondary antibody was Alexa-594-conjugated goat anti-rabbit IgG (Molecular Probes, 1:100). Nonspecific staining was ruled out by control experiments performed by preadsorbing anti-NO<sub>2</sub>Tyr with 10 mM NO<sub>2</sub>Tyr (not shown). AlexaFluor-488 phalloidin (Molecular Probes, 1 unit) was used for visualizing actin. Images were acquired on a Leitz orthoplan microscope (Leica Inc., Wetzlar, Germany) or a Leica DMIRBE inverted epifluorescence-Nomarski microscope with Leica TCS NT laser confocal optics. Apoptotic cells were visualized with the terminal deoxynucleotide transferase (TdT) FragEL DNA fragmentation kit (Oncogene) analogous to TdT-mediated nick end-labeling.

**Measurement of Plasma and Tissue NO<sub>2</sub>Tyr**—Blood was collected from healthy HbA adult volunteers and homozygous HbS patients in anticoagulated (EDTA) Vacutainers as approved by the Institutional Review Board for Human Use at the University of Alabama at Birmingham. Blood cells were removed by centrifugation, and plasma was stored at -80 °C for subsequent processing and analysis. The liver and kidneys of C57Bl/6J or knockout-transgenic SCD mice, which synthesize exclusively human Hb in the murine red blood cells (37), were dissected, weighed, and homogenized in ice-cold homogenizing buffer (50 mM K<sub>2</sub>HPO<sub>4</sub>, 80 μM leupeptin, 2.1 mM Pefabloc SC, 1 mM phenylmethylsulfonyl fluoride, 1 μg ml<sup>-1</sup> aprotinin, pH 7.4). Homogenates were centrifuged (40,000 × g, 30 min, 4 °C), and supernatants were stored at -80 °C. Plasma and tissue protein NO<sub>2</sub>Tyr was quantified by gas chromatography-MS as described previously (38). For use as an internal standard, 3-[<sup>13</sup>C<sub>6</sub>]nitrotyrosine was synthesized by the addition of 1.5 mM ONOO<sup>-</sup> to 6 mM of [<sup>13</sup>C<sub>6</sub>]tyrosine (Cambridge Isotope Laboratories) and purified and quantified via HPLC (38). Peroxynitrite was synthesized as described previously (24) and its concentration determined spectrophotometrically at 302 nm (ε<sub>M</sub> = 1670 M<sup>-1</sup> cm<sup>-1</sup>). All samples were analyzed immediately following derivatization in the electron ionization mode (EI) with a Varian GC 3800 gas chromatograph equipped with a 30 m × 0.25 mm ID fused silica capillary column having a DB-5 stationary phase and interfaced with a Varian Saturn 2000 mass spectrometer.

**Purification of Actin from Kidney and Liver**—Tissue actin purification was performed by DNase I affinity chromatography as described previously (39, 40). Briefly, 15 ml of Affi-Gel 10 (BioRad) was transferred to a Buchner funnel and washed with 3 bed volumes of cold deionized water. The gel cake was incubated with 100 mg of DNase I (Roche Diagnostics) and dissolved in 10 ml ice-cold coupling buffer (0.1 M HEPES, pH 7.4, 2 mM CaCl<sub>2</sub>) for 4 h at 4 °C. The gel slurry was loaded into a column, washed with cold deionized water, and equilibrated with buffer G (2 mM Tris-HCl, pH 7.9, 0.2 mM CaCl<sub>2</sub>, 0.2 mM ATP, and 0.2 mM dithiothreitol). Liver and kidney were dissected, weighed, and homogenized in ice-cold buffer G containing 10% formamide (v/v) (Sigma). Homogenates were centrifuged (100,000 × g, 1 h, 4 °C), and supernatants were applied to the DNase I-agarose column. The column was washed successively with buffer G, 0.2 M NH<sub>4</sub>Cl in buffer G containing 10% formamide (v/v) and with buffer G containing 10% formamide (v/v). Adsorbed actin was eluted with buffer G containing 40% formamide (v/v). Pilot studies using actin treated with 0.3 mM ONOO<sup>-</sup> showed similar chromatographic behavior of native actin.

**Western Blot Analysis and Immunoprecipitation**—For Western blotting, mouse monoclonal anti-NO<sub>2</sub>Tyr (Cayman, 2 μg ml<sup>-1</sup>), rabbit polyclonal anti-NO<sub>2</sub>Tyr (Cayman, 2 μg ml<sup>-1</sup>), and anti-NOS2 (BD Trans-

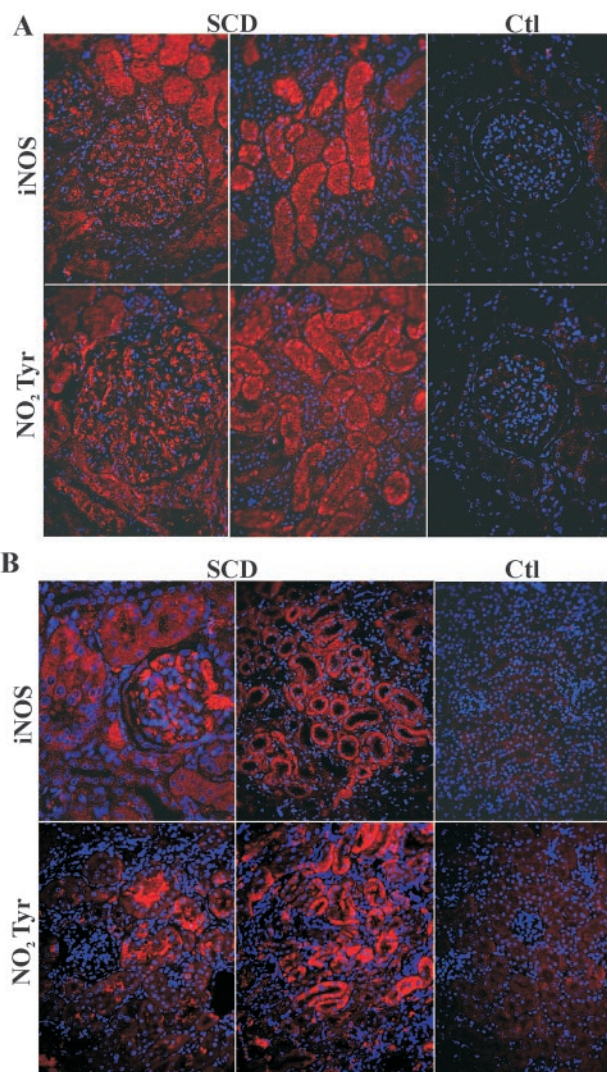


**FIG. 1. Immunofluorescent staining of NOS2 and 3-nitrotyrosine in control and sickle cell diseased renal cortex.** A, sections from sickle cell and control (Ctl) human kidney. Glomeruli and proximal and distal tubules display intense immunofluorescence for NOS2 and NO<sub>2</sub>Tyr when compared with controls. B, sections from a knockout-transgenic sickle cell and C57Bl/6J control mouse kidney. NOS2 staining is observed in the glomeruli and in tubular epithelial cells, whereas NO<sub>2</sub>Tyr immunoreactivity is localized principally to distal and proximal tubules. NOS2 and NO<sub>2</sub>Tyr staining is not evident in C57Bl/6J control sections. Nuclei are counterstained with Hoechst in all experiments.

duction Laboratories, 1:800 dilution) were used as primary antibodies. Horseradish peroxidase-conjugated goat anti-mouse IgG (Pierce, 1:10000) was used as a secondary antibody, and immunoreactive proteins were visualized by chemiluminescence (ECL reagent, Amersham Pharmacia Biotech). For immunoprecipitation, tissue homogenates were cleared with protein A-agarose (Roche Molecular Biochemicals) for 3 h at 4 °C. Supernatants were then incubated with rabbit polyclonal anti-NO<sub>2</sub>Tyr (Cayman, 5 μg ml<sup>-1</sup>) for 1 h followed by protein A-agarose incubation for 3 h at 4 °C. NO<sub>2</sub>Tyr-containing actin was immunoprecipitated from actin-enriched SCD liver and kidney extracts with a NO<sub>2</sub>Tyr affinity sorbent (Cayman, 40 μl ml<sup>-1</sup>). Immunoprecipitated proteins were washed, separated by SDS-PAGE, and visualized by GelCode Coomassie Blue stain reagent (Pierce).

**MALDI-TOF and Electrospray Mass Spectrometry**—In-gel protein digests were prepared as described previously (41, 42). Briefly, protein bands were excised from gels, destained with acetonitrile/25 mM ammonium bicarbonate (1:1, v/v), and dried. Samples were rehydrated with 12.5 ng μl<sup>-1</sup> trypsin (Promega) in 25 mM ammonium bicarbonate buffer and digested overnight at 37 °C. Peptides were extracted with acetonitrile/5% formic acid (1:1, v/v), mixed with cyano-4-hydroxycinnamic acid (Aldrich) (1:1, v/v), and spotted onto a gold-coated MALDI plate. Peptide molecular ions were analyzed in the positive ion mode

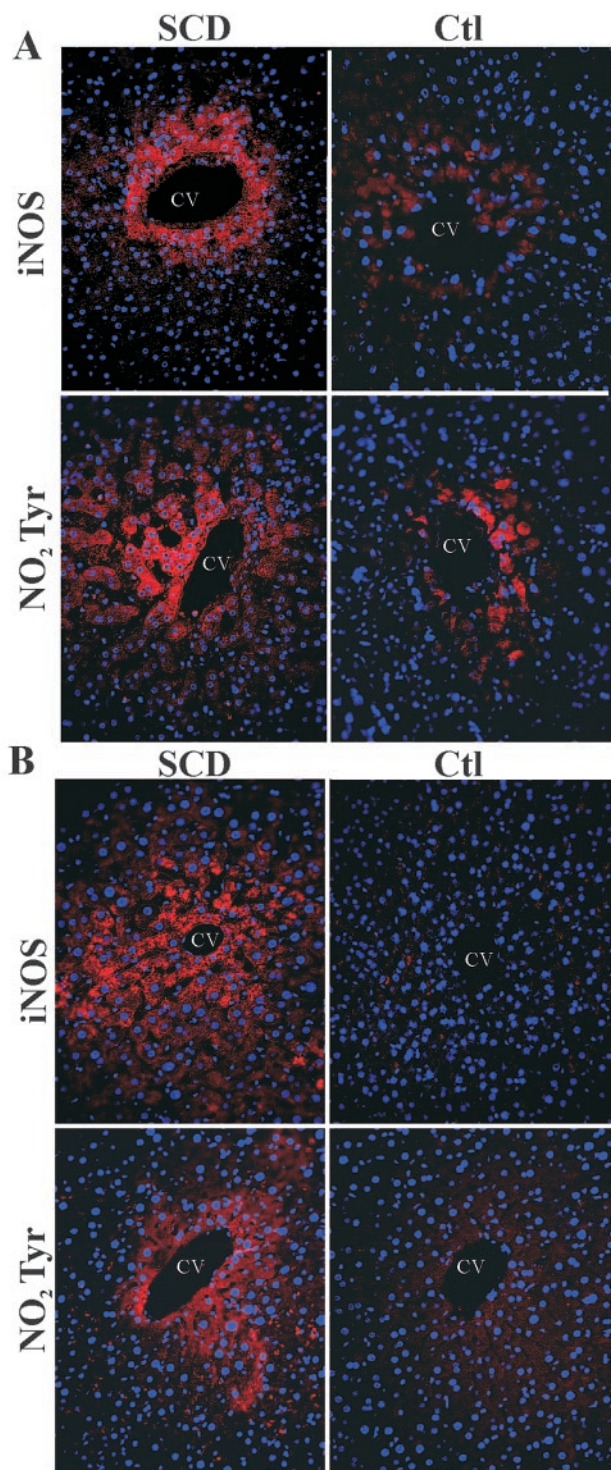


**FIG. 2. Immunofluorescent staining of NOS2 and NO<sub>2</sub>Tyr in control and sickle cell liver.** A, sections from sickle cell and control (*Ctl*) human liver. NOS2 and NO<sub>2</sub>Tyr staining is observed predominantly in the pericentral hepatocytes of SCD liver compared with controls. B, sections from knockout-transgenic sickle cell and C57Bl/6J control mouse liver. Increased NOS2 and NO<sub>2</sub>Tyr staining are localized to the pericentral hepatocytes of SCD mouse and are not evident in controls. Nuclei are counterstained with Hoechst in all experiments. CV, central vein.

using a Voyager DePro mass spectrometer (Applied Biosystems). The acceleration voltage was set at 20 kV, and 100 laser shots were summed. In some cases, purified rabbit skeletal actin (Sigma, 24  $\mu$ M) was modified minimally with 0.3 mM ONOO<sup>-</sup>, denatured with 6 M guanidine hydrochloride, and reduced with 5 mM dithiothreitol for 2 h

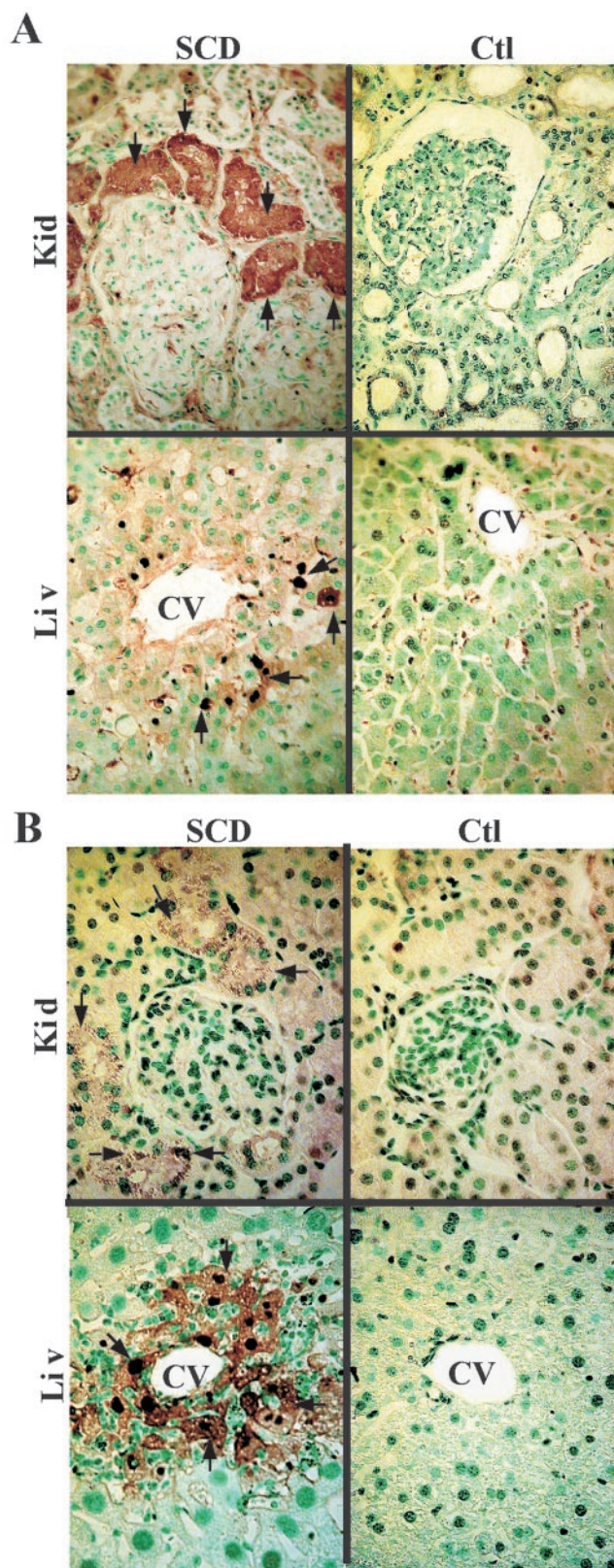


**FIG. 3. TUNEL staining in control and sickle cell kidney and liver.** Dark brown cells with pyknotic nuclei indicate positive staining for apoptosis, and green to greenish tan signifies a nonreactive cell. A, sections from control (*Ctl*) and sickle cell human kidney and liver. Apoptotic cells are seen in the tubular epithelium and glomeruli of SCD renal cortex and in pericentral hepatocytes of SCD liver. B, sections from a knockout-transgenic SCD and C57Bl/6J control mouse kidney and liver. Apoptosis is prevalent in the proximal and distal tubules of SCD kidney and in the pericentral hepatocytes of SCD liver. CV, central vein.

TABLE I  
3-Nitrotyrosine content in sickle cell disease

| Measurement                   | 3-Nitrotyrosine             |                              |
|-------------------------------|-----------------------------|------------------------------|
|                               | Control                     | SCD                          |
| Human                         |                             |                              |
| Plasma (ng/mg protein)        | 10.1 ± 3.2 (3) <sup>a</sup> | 24.7 ± 1.7 <sup>b</sup> (4)  |
| Mouse tissue                  |                             |                              |
| Plasma (ng/mg protein)        | 13.1 ± 2.2 (3)              | 37.7 ± 6.6 <sup>b</sup> (4)  |
| Liver (ng/mg protein)         | 8.2 ± 2.2 (3)               | 21.4 ± 2.6 <sup>b</sup> (5)  |
| Kidney (ng/mg protein)        | 10.0 ± 1.2 (3)              | 37.5 ± 7.8 <sup>b</sup> (4)  |
| Mouse actin-enriched fraction |                             |                              |
| Liver (μg/mg protein)         | 0.13 ± 0.03 (2)             | 0.34 ± 0.06 (3)              |
| Kidney (μg/mg protein)        | 0.17 ± 0.03 (2)             | 0.92 ± 0.08 <sup>b</sup> (3) |

<sup>a</sup> n for each measurement is in parentheses.

<sup>b</sup> p < 0.05 from control.

at 37 °C. Cysteines were alkylated with 1 mM iodoacetamide for 2 h in the dark at 25 °C. Samples were dialyzed on 10-kDa molecular mass cut-off Slide-A-Lyzer Cassettes (Pierce) against 100 mM ammonium bicarbonate, pH 8, and digested with 25 μg of sequencing grade modified trypsin (Promega). For electrospray analysis, peptide fragments were separated by reverse-phase HPLC column (300 μm × 15 cm C18 PepMap) at a flow rate of 2 μl min<sup>-1</sup> with a gradient from 20 to 100% acetonitrile, 0.1% formic acid over a period of 20 min. For both rabbit- and mouse-derived actin samples, electrospray-mass spectrometry was performed on a Q-TOF II MS (Micromass, Manchester, UK) with automatic functional switching between survey MS and MS/MS modes. A multiply charged peak above 6 counts detected in the mass spectrum was selected automatically for tandem MS analysis.

**Measurement of Actin Polymerization**—Actin was purified from rabbit hind limb, gel-filtered, and labeled with pyrenyl iodoacetamide (pyrene-labeled actin) as described previously (43, 44). In some cases control and pyrene-labeled actin were treated with 0.3 mM ONOO<sup>-</sup>, reduced with 2 mM dithiothreitol, and dialyzed against 5 mM Tris-HCl, 0.2 mM CaCl<sub>2</sub>, 0.2 mM ATP, pH 8.0. Control and nitrated actin (9.6 μM) were mixed with equimolar pyrene-conjugated G-actin (1:1, v/v), and polymer formation was monitored by pyrene actin fluorescence (45) via an automated microplate fluorescence reader (Fluostar Galaxy, BMG Laboratory Technologies) set at λ<sub>ex</sub> = 350 nm and λ<sub>em</sub> = 410 nm. Steady-state polymerization of control and nitrated actin were assayed by fluorescence intensity (λ<sub>ex</sub> = 345 nm and λ<sub>em</sub> = 407 nm) of pyrene-labeled actin in 50 mM KCl, 25 mM Hepes, 2 mM MgCl<sub>2</sub>, 0.1 mM CaCl<sub>2</sub>, 0.2 mM ATP, and 1 mM dithiothreitol. Depolymerization kinetics were measured by mixing nitrated or native pyrene-labeled F-actin with DNase I (with an actin:DNase ratio of 1:5 (mol/mol)) and monitoring fluorescence intensity as above.

## RESULTS

**Kidney and Liver NOS2 Expression and NO<sub>2</sub>Tyr Formation**—There was a strong co-distribution of NOS2 and tissue NO<sub>2</sub>Tyr immunostaining in the renal cortex of knockout-transgenic SCD mice and humans with SCD that was not evident in wild type (control) C57Bl/6J mice or healthy humans expressing HbA (Fig. 1). Distribution of NOS2 expression in SCD kidneys was in distal and proximal tubular epithelial cells and glomeruli. The proximal and distal tubules were immunoreactive for NO<sub>2</sub>Tyr in both SCD mouse and human but unlike mice, human SCD kidneys were also immunoreactive for NO<sub>2</sub>Tyr in glomeruli (Fig. 1, A and B). The expression of NOS2 in SCD human and mouse liver was localized to hepatocytes surrounding the central veins and co-distributed with NO<sub>2</sub>Tyr immunoreactivity (Fig. 2, A and B). Immunoreactive NOS2 and NO<sub>2</sub>Tyr was significantly less in control mouse and human liver (Fig. 2). Preadsorption of anti-NO<sub>2</sub>Tyr with NO<sub>2</sub>Tyr revealed that NO<sub>2</sub>Tyr immunostaining in kidney and liver sections was specific (not shown). Western blot analysis of NOS2 expression and NO<sub>2</sub>Tyr in kidney and liver homogenates revealed increased NOS2 expression and protein NO<sub>2</sub>Tyr content in SCD mice compared with controls (Fig. 4, A and B).

**Apoptosis**—TUNEL labeling showed dark brown apoptotic cells with pyknotic nuclei in the proximal and distal convoluted

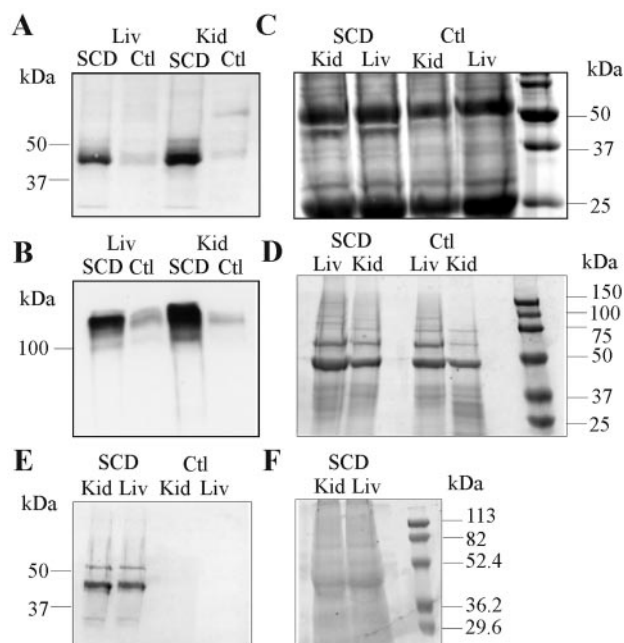
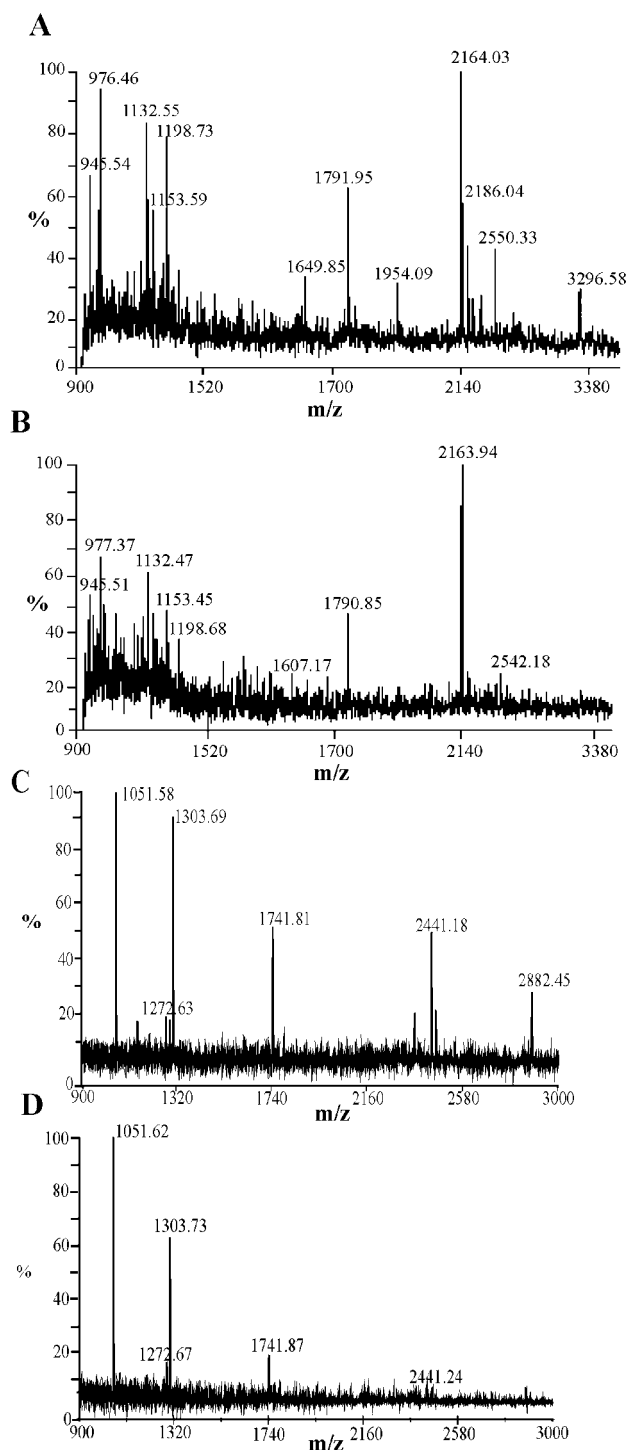


FIG. 4. SDS-PAGE and Western blot analysis of kidney and liver homogenates and immunoprecipitation pellets. A and B, kidney and liver homogenates of knockout-transgenic SCD and C57Bl/6J control mice analyzed by immunoblotting with mouse mAb against NO<sub>2</sub>Tyr (A) or NOS2 (B). C, immunoprecipitation of SCD and C57Bl/6J control (Ctl) mouse kidney (Kid) and liver (Liv) homogenates using a polyclonal NO<sub>2</sub>Tyr antibody. The immunoprecipitation pellet was separated by SDS-PAGE and visualized by Coomassie Blue staining. The nitrated protein was observed as a single 42-kDa band in SCD kidney and liver with IgG heavy (50 kDa) and light chains (25 kDa). (D) SDS-PAGE and Coomassie Blue staining of actin-enriched kidney and liver extracts obtained from SCD and C57Bl/6J control mouse. E, immunoblot analysis of actin-enriched kidney and liver extracts using a polyclonal NO<sub>2</sub>Tyr antibody. The observed NO<sub>2</sub>Tyr-containing proteins in SCD kidney and liver correspond to actin (42 kDa) and actin-associated vitamin D-binding protein (53 kDa). F, immunoprecipitation of actin-enriched SCD liver and kidney extracts with NO<sub>2</sub>Tyr affinity sorbent. The immunoprecipitation pellet was separated by SDS-PAGE and visualized by Coomassie Blue staining.

tubules and the glomeruli of SCD human kidney (Fig. 3A) and the proximal and distal tubules of SCD mouse kidney (Fig. 3B). TUNEL staining in SCD human and mouse liver was localized principally to the pericentral hepatocytes (Fig. 3, A and B).

**Plasma and Tissue NO<sub>2</sub>Tyr Concentrations**—Plasma protein NO<sub>2</sub>Tyr content was increased 2.4- and 2.8-fold over controls in SCD humans and mice, 24.7 ± 1.7 and 37.7 ± 6.6 ng/mg protein, respectively (Table I). There was also a marked difference in liver and kidney homogenate protein NO<sub>2</sub>Tyr adducts in SCD mice (21.4 ± 2.6 and 37.5 ± 7.8 ng/mg protein, respectively) versus controls (8.2 ± 2.2 and 10 ± 1.2 ng/mg protein).



**FIG. 5. MALDI-TOF MS identification of actin and vitamin D-binding protein.** The 42-kDa protein, immunoprecipitated from liver and kidney homogenates of SCD mouse via a NO<sub>2</sub>Tyr antibody, was in-gel digested and analyzed by MALDI-TOF MS. Peptide fragments from kidney (A)- and liver (B)-matched mouse actin with Mascot algorithm analysis. The NO<sub>2</sub>Tyr-containing 53-kDa band observed in actin-enriched SCD tissue extracts was in-gel digested and identified by MALDI-TOF MS. Mass fingerprint data sets obtained from SCD liver (C) and kidney (D) were analyzed using Mascot algorithm with fragment ions matching mouse vitamin D-binding protein.

The actin-enriched fraction of mouse liver and kidney showed a greater protein NO<sub>2</sub>Tyr content in both control and SCD mice compared with whole organ homogenates. Finally, there was a 17–24-fold increase in actin nitration in SCD mouse liver and kidney, respectively (Table I).

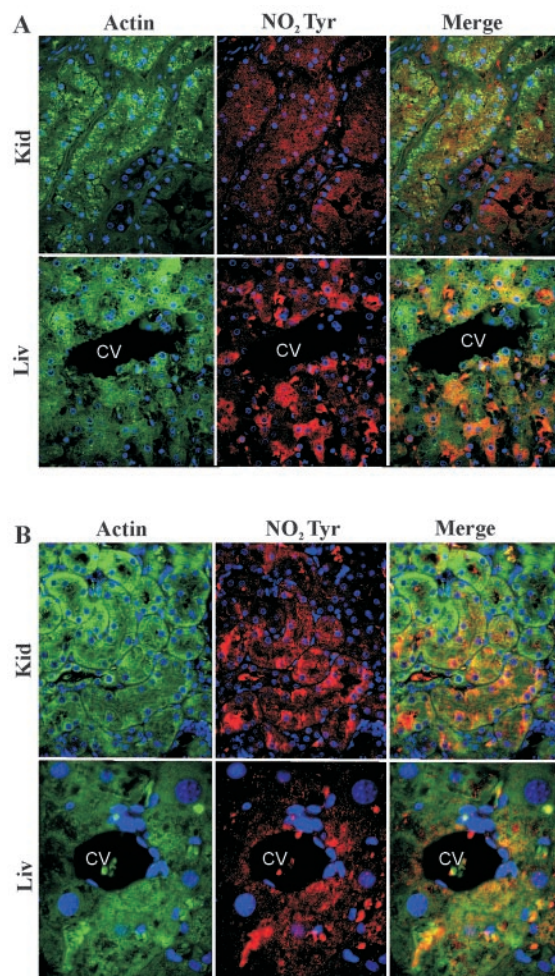


**FIG. 6. Immunohistochemical co-distribution of actin and NO<sub>2</sub>Tyr in sickle cell kidney and liver.** A, sections from sickle cell human kidney and liver. B, sections from knockout-transgenic SCD mouse kidney and liver. Tissue sections were labeled for actin (green) and NO<sub>2</sub>Tyr (red). Nuclei (blue) were counterstained with Hoechst. To assess co-distribution of actin and NO<sub>2</sub>Tyr, images were merged (orange). CV, central vein.

**Actin Nitration**—Western blot analysis of mouse kidney and liver homogenates with anti-NO<sub>2</sub>Tyr showed one predominant (42 kDa) immunoreactive band in SCD tissues compared with controls (Fig. 4A). Immunoprecipitation of kidney and liver protein extracts with polyclonal anti-NO<sub>2</sub>Tyr also revealed a NO<sub>2</sub>Tyr-containing 42-kDa protein (Fig. 4C) in SCD but not wild type mice. The 42-kDa NO<sub>2</sub>Tyr-containing protein bands for both liver and kidney were excised from gels following electrophoresis, digested with trypsin, and analyzed by MALDI-TOF mass spectrometry. Mass fingerprint data sets were analyzed using a Mascot algorithm (46) with fragment ions of *m/z* 976, 1132, 1153, 1198, and 1791 (Fig. 5, A and B) matching mouse actin with a score of 84 ( $p < 0.05$ ), well above the significance threshold of 71. Mouse liver and kidney actin were partially purified by DNase I affinity chromatography (Fig. 4D), and protein nitration was verified by immunoblotting with a polyclonal NO<sub>2</sub>Tyr antibody (Fig. 4E). The strong colocalization of actin and NO<sub>2</sub>Tyr immunoreactivity in the merged fluorescence images (Fig. 6, A and B) also further confirmed actin nitration in SCD kidney and liver. The minor NO<sub>2</sub>Tyr-containing 53-kDa band observed in actin-enriched SCD tissue extracts (Fig. 4E) was also in-gel digested and analyzed by MALDI-TOF mass spectrometry. Mass fingerprint data sets were analyzed using a Mascot algorithm (46) with

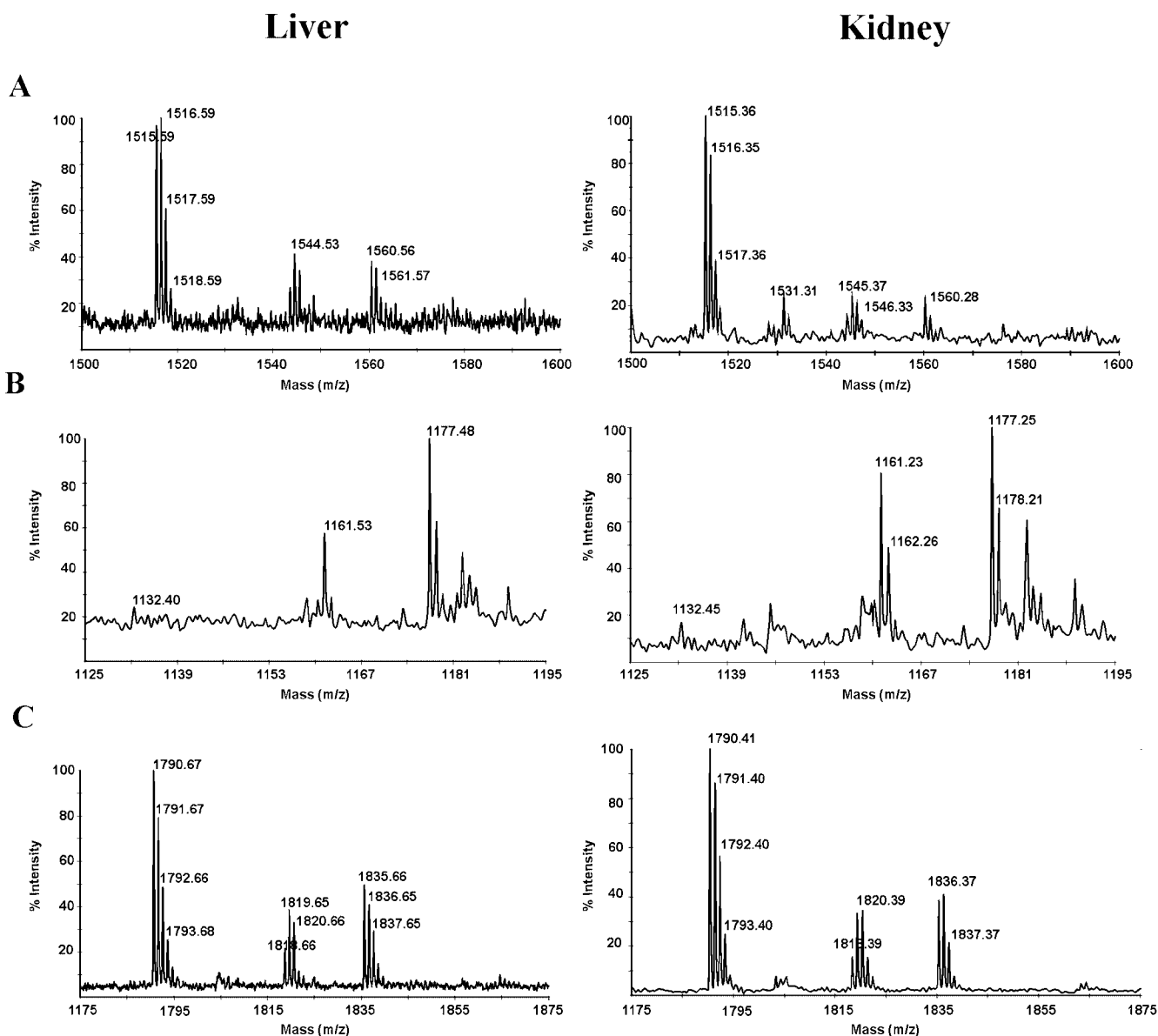


FIG. 7. MALDI-TOF MS of identification nitrated actin fragments. NO<sub>2</sub>Tyr-enriched actin fractions, obtained from actin-enriched SCD liver and kidney extracts via NO<sub>2</sub>Tyr antibody immunoprecipitation, were in-gel digested and analyzed by MALDI-TOF MS. A, MS spectrum of the nitrated tryptic fragment <sup>85</sup>IWHHTFYNELR<sup>95</sup> [M+H]<sup>+</sup> (*m/z* 1561). B, MS spectrum of the nitrated tryptic fragment <sup>197</sup>GYSFTTTAER<sup>206</sup> [M+H]<sup>+</sup> (*m/z* 1177). C, MS spectrum of the nitrated tryptic fragment <sup>239</sup>SYELPDGQVITIGNER<sup>254</sup> [M+H]<sup>+</sup> (*m/z* 1836).

ions of *m/z* 1051, 1272, 1303, 1741, 2441, and 2882 (Fig. 5, C and D) identifying G-actin-associated vitamin D-binding protein with a score of 79 ( $p < 0.05$ ).

**Identification of Specific Actin Tyrosine Residues Nitrated *in Vivo***—A NO<sub>2</sub>Tyr-enriched actin fraction from SCD mouse liver and kidney homogenates was prepared by immunoprecipitation of NO<sub>2</sub>Tyr-containing protein from the actin fraction purified by DNase I affinity chromatography (Fig. 4F). Following electrophoretic separation, the 42-kDa NO<sub>2</sub>Tyr-containing protein band was in-gel digested and analyzed by MALDI-TOF mass spectrometry and MS/MS. The observed mass fingerprint data sets for actin revealed nitration of three tyrosine residues *in vivo* (Tyr<sup>91</sup>, Tyr<sup>198</sup>, and Tyr<sup>240</sup>). The MALDI-TOF mass spectrum of the tryptic fragment corresponding to residues 85–95 (Fig. 7A) showed a +45 mass unit ion shift from *m/z* 1516 to 1561. The MS/MS spectrum of the same fragment (Fig. 8A) reflected an identical mass increase in *y*10, *y*9, *y*8, *y*7, and *y*6 daughter ions, indicative of Tyr<sup>91</sup> nitration. The MALDI-TOF spectrum of the tryptic fragment corresponding to residues

197–206 (Fig. 7B) showed a shift of +45 mass units from *m/z* 1132 to 1177, whereas the MS/MS spectrum of the same fragment (Fig. 8B) showed a *b*2 ion that shifted from *m/z* 221 to 266, identifying Tyr<sup>198</sup> as the nitrated residue. The MALDI-TOF spectrum of the tryptic fragment corresponding to residues 239–254 (Fig. 7C) showed an ion shift of +45 mass units from *m/z* 1791 to 1836, whereas the MS/MS spectrum of the same fragment (Fig. 8C) showed a *b*2 ion that shifted from *m/z* 251 to 296, revealing Tyr<sup>240</sup> as the site of nitration.

**Actin Nitration *in Vitro***—Purified rabbit muscle G-actin was utilized to analyze the influence of tyrosine nitration on the kinetics of actin polymerization, and hence it was essential to identify the sites of actin tyrosine nitration *ex vivo*. Electrospray ionization MS/MS analysis of proteolytic fragments from rabbit actin treated with 0.3 mM ONOO<sup>-</sup> revealed nitration of four residues (Tyr<sup>53</sup>, Tyr<sup>198</sup>, Tyr<sup>240</sup>, and Tyr<sup>362</sup>), with nitration of Tyr<sup>362</sup> not consistently observed in some experiments. MS/MS spectra obtained by collision-induced dissociation of [M+2H]<sup>2+</sup>-nitrated tryptic fragments resulted in dominant

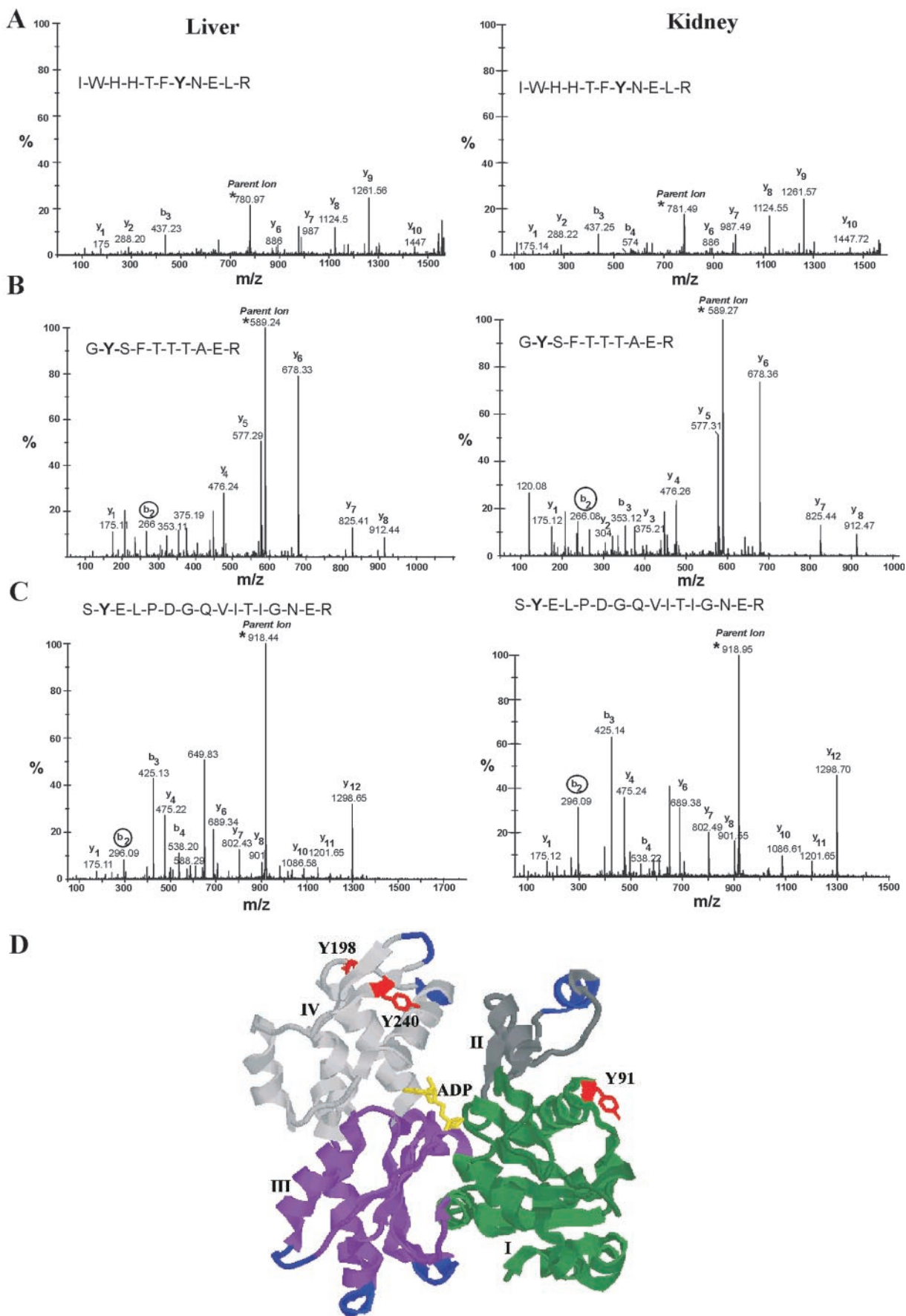


FIG. 8. MS/MS identification and representation of *in vivo* nitrated actin residues. A, MS/MS spectrum of the tryptic fragment  $^{85}\text{IWHHTFYNELR}^{95}$   $[\text{M}+2\text{H}]^{2+}$  ( $m/z$  781). B, MS/MS spectrum of the tryptic fragment  $^{197}\text{GYSFTTTAER}^{206}$   $[\text{M}+2\text{H}]^{2+}$  ( $m/z$  589). C, MS/MS spectrum of the tryptic fragment  $^{239}\text{SYELPDGQVITIGNER}^{254}$   $[\text{M}+2\text{H}]^{2+}$  ( $m/z$  918). D, ribbon representation of actin (Ref. 47; PDB Id: 1J6Z)

fragmentation at the amide bonds yielding type *b* or *y* ions (Fig 9). Again, fragment ions containing the NO<sub>2</sub> group were shifted by +45 mass units. These ions are designated by *circles* and *numbered* according to their position along the sequence (Fig. 9). The MS/MS spectrum of the tryptic fragment corresponding to residues 51–61 (parent ion, *m/z* 622.2) showed a *y*9 ion that shifted from *m/z* 996.4 to 1041.5 and a *b*3 ion that shifted from *m/z* 366.1 to 411.1, thus identifying Tyr<sup>53</sup> in the amino acid sequence DSYVGDEAQS<sup>K</sup> as the site of nitration (Fig. 9A). The MS/MS spectrum of the tryptic fragment corresponding to residues 197–206 (parent ion *m/z* 588.7) showed a *b*2 ion that shifted from *m/z* 221 to 266, identifying Tyr<sup>198</sup> in the amino acid sequence GYSFVTTAER as the nitrated residue (Fig. 9B). The MS/MS spectrum of the tryptic fragment corresponding to residues 239–254 (parent ion *m/z* 918.4) showed a *b*2 ion that shifted from *m/z* 251 to 296, revealing Tyr<sup>240</sup> in the amino acid sequence SYELPDGQVITIGNER as the site of nitration (Fig. 9C). The MS/MS spectrum of the tryptic fragment corresponding to residues 360–372 (parent ion *m/z* 773.8) showed a *y*11 ion that shifted from *m/z* 1243 to 1288, exposing Tyr<sup>362</sup> in the amino acid sequence QEYDEAGPSIVHR as the nitrated residue (Fig. 9D).

**Effect of Nitration on Actin Polymerization**—Because tyrosine residues 198 and 240 are in the region of the “pointed” end of the actin filament (47), critical concentration, a measure of actin affinity for the rapidly growing “barbed” end of the filament (48), was examined by using pyrene fluorescence emission (45). A plot of pyrenyl fluorescence *versus* actin concentration is shown in Fig. 10A. The pyrenyl fluorescence emission of nitrated G-actin was quenched by 50% compared with native G-actin, because of the broad absorption band of nitrotyrosine ( $\epsilon_{430} = 4400 \text{ M}^{-1}\text{cm}^{-1}$  (49)). Even in the presence of this quenching, a significant effect of nitration on critical concentration was observed. For native actin (*open circles*), the extrapolated critical concentration is  $89 \pm 16 \text{ nM}$ , similar to previous measurements at this ionic strength in 50 mM KCl (50). By contrast, the curve for nitrated actin extrapolated to the origin, implying a critical concentration  $< 10 \text{ nM}$ .

Polymerization of actin is accomplished in two steps, formation of relatively unstable nuclei followed by rapid elongation. The nucleation event is rate-limiting and is evidenced by a lag in formation of actin filaments during the polymerization process. The results depicted in Fig. 10A imply that nitration stabilizes interactions between the pointed end of G-actin and the barbed end of a growing actin filament. This would be expected to have two effects: 1) it should stabilize formation of actin nuclei and shorten the lag phase; and 2) it should either accelerate the rate of filament elongation or slow the rate of subunit dissociation, because the lower critical concentration implies a tighter affinity of G-actin for the barbed end. Fig. 10B shows a plot of pyrene fluorescence *versus* time for the polymerization reaction using native (*closed triangles*) and nitrated (*open boxes*) actin. Actin nitration shortens the lag phase and accelerates filament elongation. Data for both native and nitrated actin were fitted to a sum of two exponential processes, representing a lag followed by a first order increase in fluorescence. For nitrated actin, the rate constants for the lag and rising phase were 0.0032 and 0.0038 s<sup>-1</sup>, respectively, 4–7-fold faster than the corresponding values for native actin. The higher affinity of nitrated G-actin for the actin filament is also consistent with the kinetics of subunit dissociation. The addition of a 5-fold molar excess of DNase I leads to complete depolymer-

ization of the actin filament, with the rate for this process ~2-fold slower for nitrated actin (0.00029 s<sup>-1</sup>, *open boxes*) compared with native actin (0.000545 s<sup>-1</sup>, *closed triangles*, Fig. 10C).

## DISCUSSION

The repetitive episodes of tissue ischemia-reperfusion, the pro-inflammatory state in the systemic vasculature (51, 52), and the oxidative impairment of vascular NO signaling events that occur in SCD (51) all encourage the formation of secondary oxidizing and nitrating species and contribute to impaired vascular and organ function. The occurrence of xanthine oxidase-derived, O<sub>2</sub><sup>-</sup>-dependent inhibition of NO-mediated vascular relaxation in SCD vessels (53) and the elevated expression of NOS2 (54, 55) in the kidney and liver of SCD mice and human (Figs. 1 and 2) also reinforces the concept that elevated rates of production of the oxidizing and nitrating species ONOO<sup>-</sup> occurs in SCD. A major target of tissue ONOO<sup>-</sup> reactivity is with carbon dioxide (CO<sub>2</sub>) to yield the secondary nitrating species, nitrosoperoxocarbonate (ONOOCO<sub>2</sub>) (56). Tissue hypercapnia is often a consequence of impaired vascular function and is observed in SCD (57), thus creating a setting for enhanced ONOO<sup>-</sup>-mediated nitration reactions and the amplification of NOS2 expression that occurs during hypercapnia (58). Additionally, neutrophil myeloperoxidase and other heme proteins abundantly present in SCD (59) can oxidize NO<sub>2</sub><sup>-</sup> (60, 61), an NO metabolite elevated in SCD (23), to the nitrating species nitrogen dioxide (NO<sub>2</sub>). Myeloperoxidase-catalyzed protein nitration frequently displays spatial and temporal colocalization with tyrosine nitration and has been observed to occur in the vessel wall (63). Finally, the acidotic conditions present in poorly perfused tissue compartments may promote protonation of NO<sub>2</sub><sup>-</sup>, conferring a chemistry that can also result in nitrous acid (HNO<sub>2</sub>)-mediated tyrosine nitration (64). The observation of significant increases in plasma and tissue protein NO<sub>2</sub>Tyr derivatives in an animal model and clinical SCD reinforces that one or more of these oxidative inflammatory pathways are operative and are mediating pathogenic tissue responses following the post-translational nitration of structurally and functionally important target molecules.

Nitration of free and protein-associated tyrosine residues to yield NO<sub>2</sub>Tyr has been detected in multiple species, organ systems, and cell types during both acute and chronic inflammation (65). The existence of multiple distinct, yet redundant, pathways for tyrosine nitration underscores the potential significance of this process in inflammation and cell signaling. This post-translational protein modification is thus a marker of oxidative injury that is frequently linked to altered protein function during inflammatory conditions (66–68). The reversible nature of protein NO<sub>2</sub>Tyr adducts (69, 70) also implies that tyrosine nitration may not only represent a marker of reactive nitrogen species formation and altered protein function but may also evoke protein conformational changes that mimic or impact on cell signaling events such as adenylation and tyrosine phosphorylation (71).

Critical to understanding the pathogenic inflammatory reactions occurring in SCD is the observation of NOS (2) and NO<sub>2</sub>Tyr co-distribution in humans with SCD and a mouse model of SCD (Figs. 1 and 2), where liver and kidney NO<sub>2</sub>Tyr are elevated 2.6 and 3.7-fold, respectively (Table I). Immunoprecipitation and MALDI-TOF mass spectrometry-assisted identification of actin as the predominant nitrated protein in



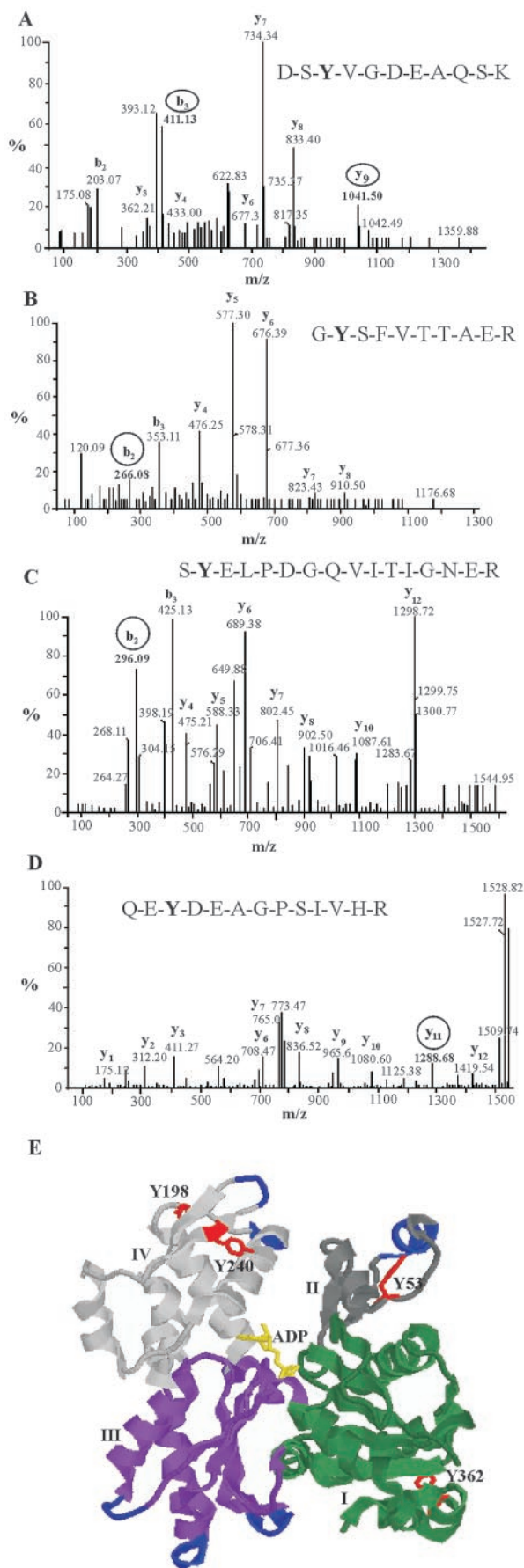


FIG. 9. Tandem  $^{32}$  MS/MS identification and representation of *in vitro* nitrated actin residues. A, MS/MS spectrum of the tryptic fragment  $^{51}$ DSYVGDEAQS $^{61}$  [ $M+2H$ ] $^{2+}$  ( $m/z$  622.2). B, MS/MS spec-

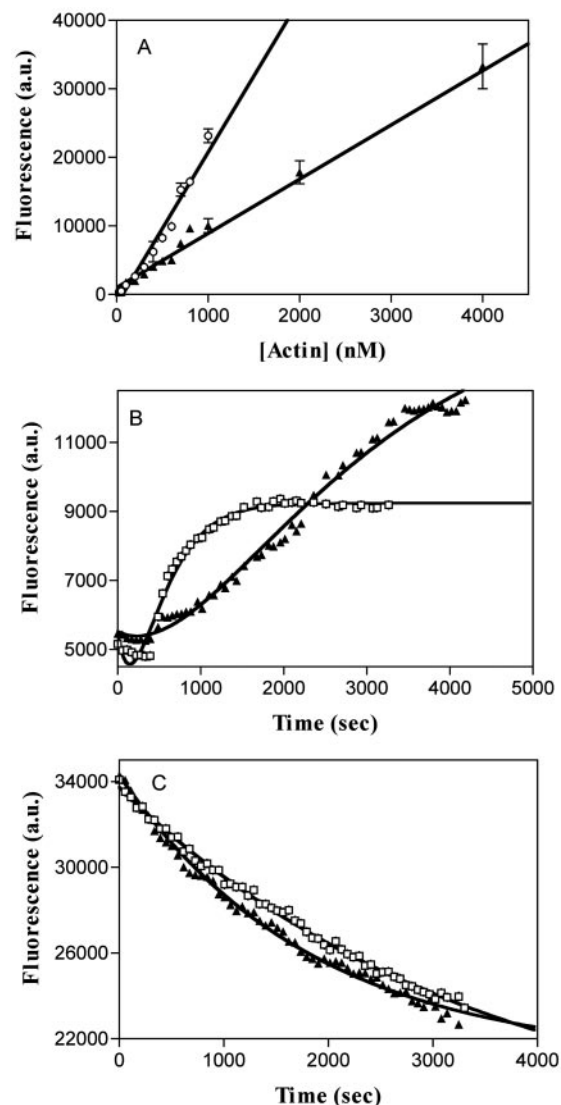


FIG. 10. Effects of nitration on actin polymerization thermodynamics and kinetics. A, critical concentration plot of native pyrene-labeled actin (open circles) compared with nitrated pyrene-labeled actin (closed triangles, 2 mol of nitrotyrosine/mol of G-actin monomer). Although the plot of fluorescence versus total actin concentration shows the inflection typical of native actin, defining a critical concentration of  $89 \pm 16$  nM, the plot for nitrated actin extrapolates to  $<10$  nM. B, kinetics of polymerization for native (closed triangles) versus nitrated (open boxes) actin (2 mol of nitrotyrosine/mol of actin). Polymerization data were fitted to a sum of two exponentials to describe a lag phase followed by a first order polymerization step. For nitrated actin, the rate constants for the lag and rising phase were  $0.0032$  and  $0.0038$   $s^{-1}$ , respectively, whereas for native actin the corresponding rates were  $0.000763$  and  $0.000564$   $s^{-1}$ . C, kinetics of depolymerization of native (closed triangles) versus nitrated (open boxes) actin filaments. Polymerized actin at a concentration of  $4$   $\mu M$  was depolymerized by the addition of  $20$   $\mu M$  DNase I. The rate of depolymerization was monitored by loss of pyrene fluorescence and followed a first order process for both preparations. The rate constants were  $0.00029$  and  $0.00055$   $s^{-1}$  for nitrated and native actin, respectively.

trum of the tryptic fragment  $^{197}$ GYSFVTTAER $^{206}$  [ $M+2H$ ] $^{2+}$  ( $m/z$  588.7). C, MS/MS spectrum of the tryptic fragment  $^{239}$ SYELPDGQVITIGNER $^{254}$  [ $M+2H$ ] $^{2+}$  ( $m/z$  918.4). D, MS/MS spectrum of the tryptic fragment  $^{360}$ QEYDEAGPSIVHR $^{372}$  [ $M+2H$ ] $^{2+}$  ( $m/z$  773.8). E, ribbon representation of actin (Ref. 47; PDB Id: 1J6Z) produced using Rasmol version 2.6. Actin subdomains are represented in green (subdomain 1), gray (subdomain 2), magenta (subdomain 3), and silver (subdomain 4). The regions contributing to longitudinal actin contacts in domains II, III, and IV are depicted in blue, and bound nucleotides are shown as yellow sticks. Nitrated tyrosine residues are shown as red sticks and are labeled with single-letter codes.

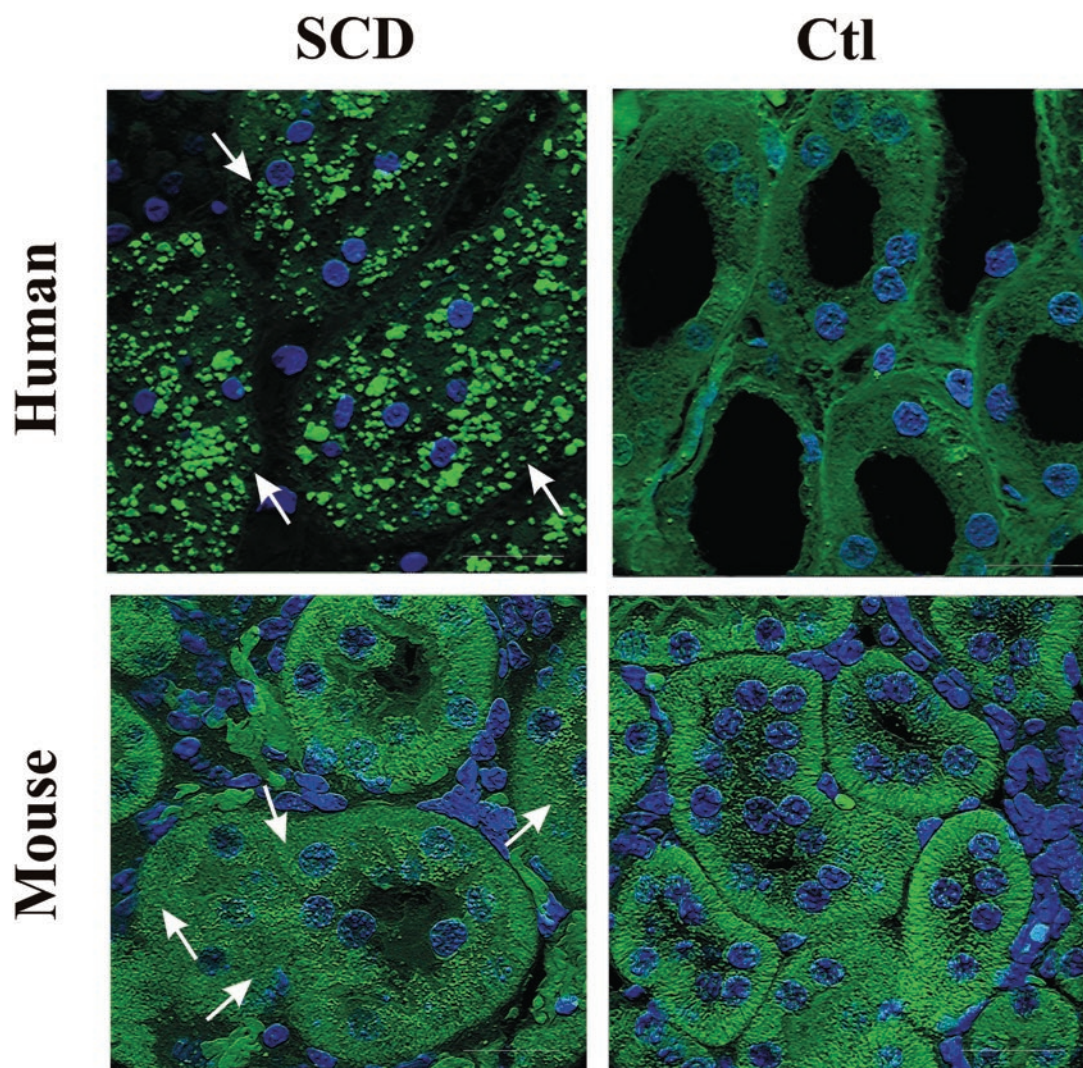


FIG. 11. **Immunofluorescent actin filament staining in control and sickle cell kidney.** F-actin prevalent in the brush border of control (*Ctrl*) human and mouse kidney tubules is disorganized and aggregated in regions indicated by *arrows* in SCD human and mouse kidney. The nuclei were counterstained with the blue fluorescent DNA stain Hoechst, and image acquisition was performed using laser confocal microscopy. CV, central vein.

the liver and kidney of SCD mouse (Figs. 4 and 5) provides critical insight into the pathogenic events to be expected from this inflammatory milieu. Particular insight in this regard is provided by the identification of specific actin tyrosine residues that are nitrated *in vivo*. Actin, one of the most abundant proteins in eukaryotic cells, constitutes 5% or more of cell protein (72) and serves with other cytoskeletal proteins such as tubulin (66) as a critical target for oxidation and nitration-induced functional impairment (73–75). As for other cytoskeletal proteins, actin contains a high percentage of tyrosine residues, many of which are crucial participants in protein-protein recognition motifs (76). The introduction of an electronegative  $\text{NO}_2$  group onto a tyrosine ring reduces the  $\text{p}K_a$  of the phenolic hydroxyl to values in the range of 6.8–7.0. If such nitrotyrosine residues were involved in intersubunit interactions, they could form ionic or hydrogen bonds with cationic residues located in the barbed end of a growing filament. This might stabilize both actin nucleus and filament formation, as evidenced by the effects of nitration on polymerization kinetics and thermodynamics (Fig. 10).

Because of the cooperative nature of actin subunit assembly (77), the functional consequences of tyrosine nitration on actin dynamics can be profound. Relatively small proportions of modified subunits could stabilize elongating filaments from fragmentation, as well as drive the equilibrium toward polymeri-

zation. Although we have not examined the effects of nitration on the severing ability of actin binding proteins such as gelsolin, it is reasonable to assume that even modest changes in intersubunit affinities will alter significantly the dynamics of actin filaments in the cell cortex. This can ultimately lead to loss of control of filament formation, with subsequent alterations in cell motility, attachment, and intracellular transport. Interestingly, we observed that the extent and sites of F- and G-actin tyrosine nitration by  $\text{ONOO}^-$  were similar (not shown), suggesting that minimal or no steric hindrance exists for the readily diffusible species that mediate nitration of either monomeric or polymerized actin. Confocal microscopy images of tissue actin distribution and morphology strongly affirm this influence of tyrosine nitration on actin polymerization properties, by reflecting a disorganized actin assembly in regions of both mouse and human SCD kidney where nitrotyrosine-containing actin was localized (Fig. 11).

A dynamic network of cytoskeletal actin is required for cell function by compartmentalizing metabolic pathways (78), promoting intracellular motility (79), and maintaining a dynamic cytoskeleton (80). The organization of actin filaments is also necessary for a direct physical link between the extracellular matrix and the cytoskeleton (81). Importantly, multiple stimuli for actin filament depolymerization will induce apoptosis (62, 82,

83). The ability of actin tyrosine nitration to alter actin polymerization (75) thus also links actin nitration with the enhanced apoptosis observed in regions of NO<sub>2</sub>Tyr immunoreactivity in the liver and kidney of SCD mouse and human (Fig. 3).

In summary, we have observed that an oxidative inflammatory milieu exists in the vasculature, kidney, and liver of SCD patients, with NO-mediated nitration reactions catalyzing the post-translational modification and functional impairment of a key cell cytoskeletal protein, actin. In addition to adversely affecting vascular function, the selective nitration of liver and kidney actin tyrosine residues can also lead to the apoptotic cell death and loss of organ function observed in SCD.

**Acknowledgments**—We appreciate the insights and assistance provided by Drs. Phil Allen, Denyse Thornley-Brown, Elizabeth Lowenthal, Phil Chumley, and Scott Sweeney.

## REFERENCES

- Pham, P. T., Pham, P. C., Wilkinson, A. H. & Lew, S. Q. (2000) *Kidney Int.* **57**, 1–8
- Bauer, T. W., Moore, G. W. & Hutchins, G. M. (1980) *Am. J. Med.* **69**, 833–837
- Johnson, C. S., Omata, M., Tong, M. J., Simmons, J. F., Jr., Weiner, J. & Tatter, D. (1985) *Medicine* **64**, 349–356
- Zweier, J. L., Kuppusamy, P., Williams, R., Rayburn, B. K., Smith, D., Weisfeldt, M. L. & Flaherty, J. T. (1989) *J. Biol. Chem.* **264**, 18890–18895
- Henry, T. D., Archer, S. L., Nelson, D., Weir, E. K. & From, A. H. (1990) *Circ. Res.* **67**, 1453–1461
- Zhou, W., Zhang, Y., Hosch, M. S., Lang, A., Zwacka, R. M. & Engelhardt, J. F. (2001) *Hepatology* **33**, 902–914
- Paller, M. S., Weber, K. & Patten, M. (1998) *Ren. Fail.* **20**, 459–469
- Engerson, T. D., McKelvey, T. G., Rhyne, D. B., Boggio, E. B., Snyder, S. J. & Jones, H. P. (1987) *J. Clin. Invest.* **79**, 1564–1570
- Wallace, D. C. (1999) *Science* **283**, 1482–1488
- Werns, S. W. & Lucchesi, B. R. (1988) *Free Radic. Biol. Med.* **4**, 31–37
- Lucchesi, B. R. (1990) *Am. J. Cardiol.* **65**, 141–231
- Tilney, N. L., Paz, D., Ames, J., Gasser, M., Laskowski, I. & Hancock, W. W. (2001) *Transplant. Proc.* **33**, 843–844
- Carden, D. L. & Granger, D. N. (2000) *J. Pathol.* **190**, 255–266
- Collard, C. D. & Gelman, S. (2001) *Anesthesiology* **94**, 1133–1138
- Isobe, M., Katsuramaki, T., Hirata, K., Kimura, H., Nagayama, M. & Matsuno, T. (1999) *Transplantation* **68**, 803–813
- Isobe, M., Katsuramaki, T., Kimura, H., Nagayama, M., Matsuno, T., Yagihashi, A. & Hirata, K. (2000) *Transplant. Proc.* **32**, 1650–1652
- Yu, L., Gengaro, P. E., Niederberger, M., Burke, T. J., Schrier, R. W. (1994) *Proc. Natl. Acad. Sci. U. S. A.* **91**, 1691–1695
- Wildhirt, S. M., Suzuki, H., Wolf, W. P., Dudek, R., Horstman, D., Weismueller, S. & Reichart, B. (1996) *Biochem. Biophys. Res. Commun.* **227**, 328–333
- Lee, V. G., Johnson, M. L., Baust, J., Laubach, V. E., Watkins, S. C. & Billiar, T. R. (2001) *Shock* **16**, 355–360
- Ling, H., Gengaro, P. E., Edelstein, C. L., Martin, P. Y., Wangsiripaisan, A., Nemenoff, R. & Schrier, R. W. (1998) *Kidney Int.* **53**, 1642–1646
- Ling, H., Edelstein, C., Gengaro, P., Meng, X., Lucia, S., Knotek, M., Wangsiripaisan, A., Shi, Y. & Schrier, R. (1999) *Am. J. Physiol.* **277**, F383–F390
- Vasquez-Vivar, J., Kalyanaram, B., Martasek, P., Hogg, N., Masters, B. S., Karoui, H., Tordo, P. & Pritchard, K. A., Jr. (1998) *Proc. Natl. Acad. Sci. U. S. A.* **95**, 9220–9225
- Rees, D. C., Cervi, P., Grimwade, D., O'Driscoll, A., Hamilton, M., Parker, N. E. & Porter, J. B. (1995) *Br. J. Haematol.* **91**, 834–837
- Beckman, J. S., Beckman, T. W., Chen, J., Marshall, P. A. & Freeman, B. A. (1990) *Proc. Natl. Acad. Sci. U. S. A.* **87**, 1620–1624
- Beckman, J. S., Ye, Y. Z., Anderson, P. G., Chen, J., Accavitti, M. A., Tarpey, M. M. & White, C. R. (1994) *Biol. Chem. Hoppe-Seyler* **375**, 81–88
- Haddad, I. Y., Pataki, G., Hu, P., Galliani, C., Beckman, J. S. & Matalon, S. (1994) *J. Clin. Invest.* **94**, 2407–2413
- Kooy, N. W., Royall, J. A., Ye, Y. Z., Kelly, D. R. & Beckman, J. S. (1995) *Am. J. Respir. Crit. Care Med.* **151**, 1250–1254
- Ottesen, L. H., Harry, D., Frost, M., Davies, S., Khan, K., Halliwell, B. & Moore, K. (2001) *Free Radic. Biol. Med.* **31**, 790–798
- Kooy, N. W., Lewis, S. J., Royall, J. A., Ye, Y. Z., Kelly, D. R. & Beckman, J. S. (1997) *Crit. Care Med.* **25**, 812–819
- Miller, M. J., Thompson, J. H., Zhang, X. J., Sadowska-Krowicka, H., Kakkis, J. L., Munshi, U. K., Sandoval, M., Rossi, J. L., Eloby-Childress, S., Beckman, J. S., Ye, Y. Z., Roddi, C. P., Manning, P. T., Currie, M. G. & Clark, D. A. (1995) *Gastroenterology* **109**, 1475–1483
- Kaur, H. & Halliwell, B. (1994) *FEBS Lett.* **350**, 9–12
- Bian, K., Davis, K., Kuret, J., Binder, L. & Murad, F. (1999) *Am. J. Physiol.* **277**, F33–F40
- MacMillan-Crow, L. A., Crow, J. P., Kerby, J. D., Beckman, J. S. & Thompson, J. A. (1996) *Proc. Natl. Acad. Sci. U. S. A.* **93**, 11853–11858
- Good, P. F., Werner, P., Hsu, A., Olanow, C. W. & Perl, D. P. (1996) *Am. J. Pathol.* **149**, 21–28
- Crow, J. P., Sampson, J. B., Zhuang, Y., Thompson, J. A. & Beckman, J. S. (1997) *J. Neurochem.* **69**, 1936–1944
- Aulak, K. S., Miyagi, M., Yan, L., West, K. A., Massillon, D., Crabb, J. W. & Stuehr, D. J. (2001) *Proc. Natl. Acad. Sci. U. S. A.* **98**, 12056–12061
- Ryan, T. M., Ciavatta, D. J. & Townes, T. M. (1997) *Science* **278**, 873–876
- Frost, M. T., Halliwell, B. & Moore, K. P. (2000) *Biochem. J.* **345**, 453–458
- Zechel, K. (1980) *Eur. J. Biochem.* **110**, 343–348
- Kron, S. J., Drubin, D. G., Botstein, D. & Spudich, J. A. (1992) *Proc. Natl. Acad. Sci. U. S. A.* **89**, 4466–4470
- Rosenfeld, J., Capdevielle, J., Guillemot, J. C. & Ferrara, P. (1992) *Anal. Biochem.* **203**, 173–179
- Hellman, U., Wernstedt, C., Gonez, J. & Heldin, C. H. (1995) *Anal. Biochem.* **224**, 451–455
- Spudich, J. A. & Watt, S. (1971) *J. Biol. Chem.* **246**, 4866–4871
- Pollard, T. D. (1984) *J. Cell Biol.* **99**, 769–777
- Cooper, J. A. (1992) in *The Cytoskeleton: A Practical Approach* (Carraway, K. L., and Carraway, C. A. C., eds) pp. 74–71, IRL Press, New York
- Perkins, D. N., Pappin, D. J., Creasy, D. M. & Cottrell, J. S. (1999) *Electrophoresis* **20**, 3551–3567
- Otterbein, L. R., Graceffa, P. & Dominguez, R. (2001) *Science* **293**, 708–711
- Carlier, M. F. & Pantaloni, D. (1997) *J. Mol. Biol.* **269**, 459–467
- Gow, A., McClelland, M., Garner, S. E., Malcolm, S. & Ischiropoulos, H. (1998) *Methods in Molecular Biology Series: Nitric Oxide Protocols* (Titheradge, M. A., ed) pp. 291–293, Humana Press, Totowa, NJ
- Pollard, T. D., Blanchoin, L. & Mullins, R. D. (2000) *Annu. Rev. Biophys. Biomol. Struct.* **29**, 545–576
- Osarogiabon, U. R., Choong, S., Belcher, J. D., Vercellotti, G. M., Paller, M. S. & Hebbel, R. P. (2000) *Blood* **96**, 314–320
- Kaul, D. K. & Hebbel, R. P. (2000) *J. Clin. Invest.* **106**, 411–420
- Aslan, M., Ryan, T. M., Adler, B., Townes, T. M., Parks, D. A., Thompson, A. J., Tousson, A., Gladwin, M. T., Patel, R. P., Tarpey, M. M., Batinic-Haberle, I., White, R. C. & Freeman, B. A. (2001) *Proc. Natl. Acad. Sci. U. S. A.* **98**, 15215–15220
- Osei, S. Y., Ahima, R. S., Fabry, M. E., Nagel, R. L. & Bank, N. (1996) *Blood* **88**, 3583–3588
- Bank, N., Aynedjian, H. S., Qiu, J. H., Osei, S. Y., Ahima, R. S., Fabry, M. E. & Nagel, R. L. (1996) *Kidney Int.* **50**, 184–189
- Radi, R., Denicola, A. & Freeman, B. A. (1999) *Methods Enzymol.* **301**, 353–367
- Maitre, B., Habibi, A., Roudot-Thoraval, F., Bachir, D., Belghiti, D. D., Galacteros, F. & Godeau, B. (2000) *Chest* **117**, 1386–1392
- Lang, J. D. Jr., Chumley, P., Eiserich, J. P., Estevez, A., Bamberg, T., Adhimi, A., Crow, J. & Freeman, B. A. (2000) *Am. J. Physiol.* **279**, L994–L1002
- Nath, K. A., Grande, J. P., Haggard, J. J., Croatt, A. J., Katusic, Z. S., Solovey, A. & Hebbel, R. P. (2001) *Am. J. Pathol.* **158**, 893–903
- Eiserich, J. P., Hristova, M., Cross, C. E., Jones, A. D., Freeman, B. A., Halliwell, B. & van der Vliet, A. (1998) *Nature* **391**, 393–397
- Eiserich, J. P., Baldus, S., Brennan, M., Ma, W., Zhang, C., Tousson, A., Castro, L., Lusic, A. J., White, R. C., Nauseef, W. & Freeman, B. A. (2002) *Science* **296**, 2391–2394
- Suarez-Huerta, N., Mosselmans, R., Dumont, J. E., & Robaye, B. (2000) *J. Cell. Physiol.* **184**, 239–245
- Baldus, S., Eiserich, J. P., Alireza, M., Castro, L., Figueroa, M., Chumley, P., Ma, W., Tousson, A., White, R. C., Bullard, D. C., Brennan, M., Lusic, A. J., Moore, K. P. & Freeman, B. A. (2001) *J. Clin. Invest.* **108**, 1759–1770
- Knowles, M. E., McWeeny, D. J., Couchman, L. & Thorogood, M. (1974) *Nature* **247**, 288–289
- Greenacre, S. A. & Ischiropoulos, H. (2001) *Free Radic. Res.* **34**, 541–581
- Eiserich, J. P., Estevez, A. G., Bamberg, T. V., Ye, Y. Z., Chumley, P. H., Beckman, J. S. & Freeman, B. A. (1999) *Proc. Natl. Acad. Sci. U. S. A.* **96**, 6365–6370
- MacMillan-Crow, L. A., Crow, J. P. & Thompson, J. A. (1998) *Biochemistry* **37**, 1613–1622
- Cassina, A. M., Hodara, R., Souza, J. M., Thomson, L., Castro, L., Ischiropoulos, H., Freeman, B. A. & Radi, R. (2000) *J. Biol. Chem.* **275**, 21409–21415
- Kamisaki, Y., Wada, K., Bian, K., Balabanli, B., Davis, K. L., Martin, E., Behbod, F., Lee, Y. C. & Murad, F. (1998) *Proc. Natl. Acad. Sci. U. S. A.* **95**, 11584–11589
- Davis, K. L., Martin, E., Turko, I. V. & Murad, F. (2001) *Annu. Rev. Pharmacol. Toxicol.* **41**, 203–236
- Berlett, B. S., Levine, R. L. & Stadtman, E. R. (1998) *Proc. Natl. Acad. Sci. U. S. A.* **95**, 2784–2789
- Sheterline, P. & Sparrow, J. C. (1994) *Protein Profile* **1**, 1–121
- Hinshaw, D. B., Armstrong, B. C., Burger, J. M., Beals, T. F. & Hyslop, P. A. (1988) *Am. J. Pathol.* **132**, 479–488
- Hinshaw, D. B., Burger, J. M., Beals, T. F., Armstrong, B. C. & Hyslop, P. A. (1991) *Arch. Biochem. Biophys.* **288**, 311–316
- Banan, A., Fields, J. Z., Zhang, Y. & Keshavarzian, A. (2001) *Am. J. Physiol.* **280**, G1234–G1246
- McGough, A. (1998) *Curr. Opin. Struct. Biol.* **8**, 166–176
- Erickson, H. P. (1989) *J. Mol. Biol.* **206**, 465–474
- Hennessey, E. S., Drummond, D. R., & Sparrow, J. C. (1993) *Biochem. J.* **291**, 657–671
- Weeds, A. G., Gooch, J., Hawkins, M., Pope, B., & Way, M. (1991) *Biochem. Soc. Trans.* **19**, 1016–1020
- Way, M. & Weeds, A. (1990) *Nature* **344**, 292–294
- Maniotis, A. J., Chen, C. S. & Ingber, D. E. (1997) *Proc. Natl. Acad. Sci. U. S. A.* **94**, 849–854
- Re, F., Zanetti, A., Sironi, M., Polentarutti, N., Lanfrancone, L., Dejana, E. & Colotta, F. (1994) *J. Cell Biol.* **127**, 537–546
- Martin, S. S. & Leder, P. (2001) *Mol. Cell. Biol.* **21**, 6529–6536